NPL Report MATC(A)68

Project MMS11
Report No 2

Models for Predicting Deformation and Failure In Adhesives and Polymer Matrix Composites

G D Dean and W R Broughton

February 2002

NPL Report MATC(A)68
February 2002

Models for Predicting Deformation and Failure In Adhesives and Polymer Matrix Composites

G D Dean and W R Broughton
NPL Materials Centre
National Physical Laboratory
Teddington, Middlesex
TW11 0LW, UK

ABSTRACT

This report provides an overview of predictive models for determining deformation and failure behaviour of toughened adhesives and polymer matrix composites (PMCs) under monotonic, cyclic and creep loading conditions. The report describes a new model for characterising the behaviour of rubber-toughened adhesives. This model, which accounts for the influence of rubber particle cavitation on the yield behaviour of adhesives, has been adopted for use with the finite element software package ABAQUS. Modelling non-linear creep in adhesives through the use of a model for time-dependent plasticity is also discussed. Results from failure studies conducted on different adhesive joints under monotonic loading have been included as part of the assessment on the validity of various criteria for predicting failure. The report reviews physics/mechanistic, fracture mechanics and non-mechanistic (i.e. statistical and empirical) based theories that are used to predict the onset and propagation of damage, and subsequent deterioration in thermo-elastic properties of composite laminates. It also includes three-dimensional laminate analysis.

The report was prepared as part of the research undertaken at NPL for the Department of Trade and Industry funded project on "Measurements for Materials Systems (MMS) Programme - Design for Fatigue and Creep in Joined Systems".

ISSN 1473 - 2734

National Physical Laboratory
Teddington, Middlesex, UK, TW11 0LW

Approved on behalf of Managing Director, NPL, by Dr C Lea,
Head of NPL Materials Centre.

CONTENTS

1. INTRODUCTION

In the design of a bonded structure for mechanical performance, materials models are needed to enable predictions of stress and strain distributions, and the onset and propagation of failure. Predictions of stress and strain distributions are required to reveal the deformation of the component under an applied load and also to indicate stress and strain levels in regions of stress concentration in the adhesive layer and the substrate where failure will initiate. The availability of failure criteria for both materials will then allow the conditions under which failure will initiate to be determined. Finite element analysis (FEA) is a versatile tool for calculating stress and strain distributions in bonded joints and enables the influence of geometrical details (e.g. adhesive fillets) on stress and strain levels to be taken into account.

Models (or constitutive laws) that describe the deformation behaviour of a material should take into account both isotropic and anisotropic materials (e.g. fibre-reinforced polymer composites). Where the deformation is predominantly linear to failure, the deformation behaviour of composite materials can be modelled by the equations for anisotropic elasticity. In contrast, toughened adhesives are ductile materials that undergo extensive non-linear deformation through plasticity prior to failure. Elastic-plastic models usually describe the stress/strain behaviour of these materials. These were first developed for metals, but have been modified for use with plastics and other types of material. Adhesives are also viscoelastic, thus the stress and strain distributions will depend upon loading history (i.e. rate of load application or the time under load). Non-linear viscoelastic behaviour is described using elastic-plastic models by allowing parameters in the yield criterion to be time or rate dependent.

Despite these modifications, elastic-plastic models are unable to accurately account for plastic deformation in rubber-toughened adhesives without further modification. The rubber particles in this type of adhesive promote local plastic deformation in the matrix material between particles. Under stress states where there is a sufficient hydrostatic tensile component, the rubber particles cavitate, and this serves to enhance the local plasticity. Elastic-plastic models that do not take account of cavitation are unable to accurately describe deformation under a wide range of stress states. The accuracy, obtained with these models, of stress and strain predictions in the adhesive layer in a bonded joint is therefore uncertain, and different models give widely different predicted values especially in regions of stress and strain concentration. This lack of confidence in the predictive accuracy of available models has hindered the development of a failure criterion for adhesive joints based on a critical level of some component of stress or strain needed to initiate a crack.

The prediction of static strength, progressive damage formation, the time-to-failure and the time dependence of residual strength of fibre-reinforced polymer composites is a difficult task. Failure in these multi-component systems (i.e. fibre, matrix and interface) tends to consist of a sequence of localised, strongly interactive, damage events (e.g. matrix cracking. fibre breakage and fibre splitting). The accumulative effect of these local events leads to progressive loss in stiffness and strength and eventual catastrophic failure of the material. The diversity of material formats and processing routes associated with composite materials also means that it is highly unlikely that any one model will be universally applicable to all composite materials or loading conditions. Physics/mechanistic and non-mechanistic (empirical and phenomenological/statistical) based theories abound in the literature. A number of these are being used with mixed success to predict static strength and time dependent degradation of material properties of composite laminates under cyclic and creep loading conditions.

The report examines models used to describe deformation behaviour of toughened adhesives and polymer matrix composites (PMCs) will be briefly introduced. A new model will also be described that takes account of the influence of rubber particle cavitation on the yield behaviour of adhesives. This model was developed in a previous project and has been coded as a UMAT (user defined materials model) for use with the FE software package ABAQUS. The results of failure studies of some adhesive joints under monotonic loading will be outlined and used to draw some broad conclusions regarding the validity of various criteria for predicting failure. The report reviews physics/mechanistic, fracture mechanics, statistical and empirical based theories for predicting the onset and propagation of damage, and subsequent deterioration in thermo-elastic properties of composite laminates under creep and fatigue. The review forms part of the Engineering Industries Directorate of the United Kingdom Department of Trade and Industry project on "Measurements for Materials Systems (MMS) Programme - Design for Fatigue and Creep in Joined Systems (MMS11)".

The report consists of seven sections (including the Introduction). Sections 2 and 3 examine modelling of non-linear deformation in ductile adhesives and non-linear creep deformation of polymers, respectively. Classical laminate analysis is covered in Section 4. Section 5 examines models for predicting failure in adhesives and Section 6 provides an assessment of models for determining static strength, creep and fatigue performance of composite laminates. Concluding remarks are presented in Section 7. Appendix 1 presents maximum principal stress contour plots for a scarf joint obtained using FEA for different material models.

2. MODELLING NON-LINEAR DEFORMATION IN DUCTILE ADHESIVES

A stress/strain curve for a typical rubber toughened epoxy adhesive is shown in Figure 1 obtained under tensile loading at a constant deformation rate. The adhesive has been tested at a temperature well below its glass-to-rubber transition temperature $\mathbf{T_g}$ so the material is glassy. The non-linear behaviour of glassy polymers is generally interpreted as enhanced viscoelastic deformation arising from an increase in molecular mobility caused by the application of stresses above the limit for linear behaviour. At these stress levels, relaxation times are reduced leading to enhanced creep and stress relaxation (see Section 3). Satisfactory models of this non-linear viscoelasticity have yet to be developed, and FE packages generally consider material non-linearity in rigid materials in terms of elastic-plastic models. With elastic-plastic models, calculations of stress and strain distributions at low strains are based on linear elasticity as described in Section 2.2. The onset of non-linearity is then ascribed to plastic deformation and occurs at a stress level regarded as the first yield stress. The subsequent increase in stress with strain is associated with the effects of strain hardening. In this non-linear region, the total strain $\boldsymbol{\varepsilon}$ is considered to be the sum of a recoverable elastic component $\boldsymbol{\varepsilon_{ij}^{e}}$ and a plastic component $\boldsymbol{\varepsilon_{ij}^{p}}$, which is non-recoverable, as shown below:

$$\varepsilon_{ij} = \varepsilon_{ij}^{e} + \varepsilon_{ij}^{p} \qquad (1)$$

Stress analysis calculations then involve the use of multiaxial yield criteria and a flow law. The yield criterion relates components of the applied stress field to material parameters after the onset of yielding. The material parameters will depend upon the plastic strain for a strain hardening material. This is a material having a range of yield stress varying from an initial value $\boldsymbol{\sigma_y}$, marking the onset of non-linearity, to a maximum value corresponding to the flow region (see Figure 1).

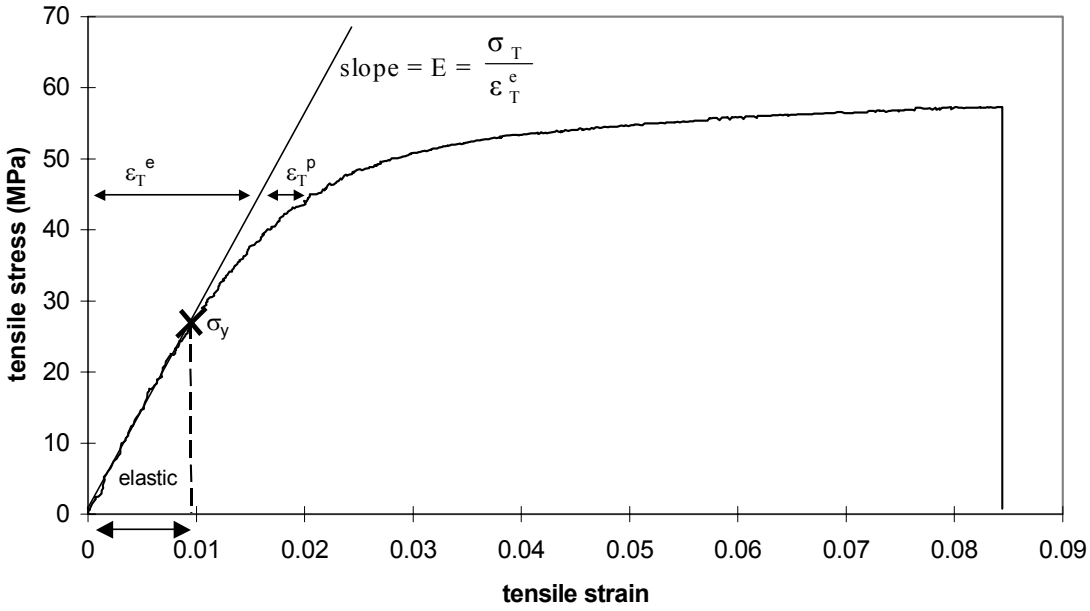

Figure 1: Tensile stress/strain curve for the rubber-toughened epoxy adhesive.

The calculation of plastic strain components is achieved in plasticity theory using a flow rule, which relates increments of plastic strain to a plastic flow potential. If the flow behaviour for a particular material is such that the flow potential can be identified with the yield function then this is termed associated flow. In general, this will be an approximation and additional information is required to characterise non-associated flow.

In order to calculate some of the parameters in elastic-plastic models, it is necessary to select stress values from tests under different stress states. The selection of these stresses requires the definition of an effective plastic strain so that stress values can be identified at the same effective plastic strain in each test (see Figure 2).

2.1 VON MISES YIELD CRITERION

The most simple yield criterion interprets yielding as a purely shear deformation process which occurs when the effective shear stress $\boldsymbol{\sigma_e}$ reaches a critical value. This effective stress is defined in terms of principal stress components $\boldsymbol{\sigma_i}$ **(i = 1, 2 or 3)** by:

$$\sigma_e = \left\{\tfrac{1}{2}\left[(\sigma_1 - \sigma_2)^2 + (\sigma_2 - \sigma_3)^2 + (\sigma_3 - \sigma_1)^2\right]\right\}^{1/2} \qquad (2)$$

The von Mises criterion then relates $\boldsymbol{\sigma_e}$ to the yield stress in tension $\boldsymbol{\sigma_T}$ by:

$$\sigma_e = \sigma_T \qquad (3)$$

The tensile yield stress $\boldsymbol{\sigma_T}$ is now a material parameter and has a minimum value, which denotes the limit of elastic behaviour and the start of plastic deformation (see Figure 1) and will increase with tensile plastic strain $\boldsymbol{\varepsilon_T^p}$. The function $\boldsymbol{\sigma_T(\varepsilon_T^p)}$ is called the tensile strain hardening function. An example is given in Figure 2 for a rubber-toughened epoxy adhesive.

Tests on adhesives under additional stress states such as shear and compression (see Figure 2) reveal that yielding is sensitive to the hydrostatic component of stress in addition to the shear component. The von Mises criterion is therefore not realistic, and alternative criteria are considered next.

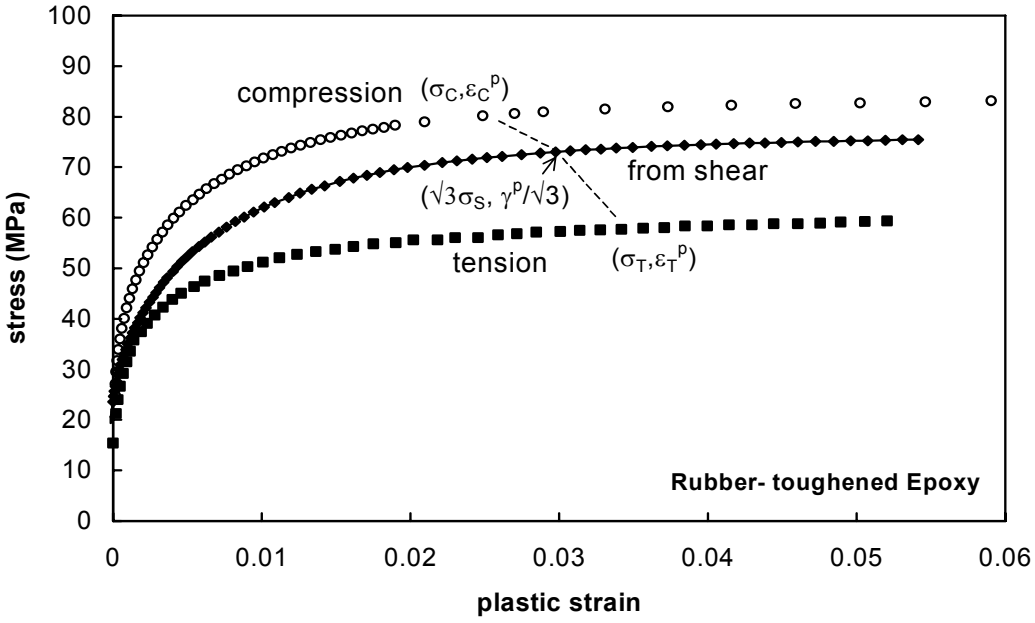

Figure 2: Comparison of stress/plastic strain curves determined under uniaxial tension, shear and uniaxial compression for the determination of stresses at the same effective plastic strain. Stresses and strains from shear data have been scaled as shown to facilitate comparisons between the curves.

2.2 LINEAR DRUCKER-PRAGER YIELD CRITERION

A simple modification of the von Mises criterion that includes hydrostatic stress sensitivity follows from Equation (3):

$$\sigma_e = \sigma_o - \mu\sigma_m \tag{4}$$

where σ_o is the material parameter, which is now related to the shear yield stress σ_S by:

$$\sigma_o = \sqrt{3}\,\sigma_S \tag{5}$$

and σ_m is the hydrostatic stress given in terms of principal stresses by:

$$\sigma_m = \tfrac{1}{3}(\sigma_1 + \sigma_2 + \sigma_3) \tag{6}$$

Equation (4) is identical to the linear Drucker-Prager model in ABAQUS. The parameter μ characterises the sensitivity of yielding to hydrostatic stress. A value for μ can be determined from tests under two different stress states.

2.3 EXPONENT DRUCKER-PRAGER CRITERION

Although the linear Drucker-Prager yield criterion includes some sensitivity of yielding to the hydrostatic stress, it is not able to describe behaviour with any accuracy under stress states in which there is a high component of hydrostatic tension. Such stress states are common locally in adhesive bonds because of the high constraint imposed by the adherend under forces directed normal to the interface. An alternative criterion is significantly more accurate under these conditions and is often written in the form:

$$\sigma_e^2 = \lambda\sigma_T^2 - 3(\lambda-1)\sigma_T\,\sigma_m \tag{7}$$

where λ is another hydrostatic stress sensitivity parameter. This criterion is implemented in ABAQUS as the exponent Drucker-Prager model with the exponent parameter of 2.

2.4 A YIELD CRITERION FOR RUBBER TOUGHENED ADHESIVES

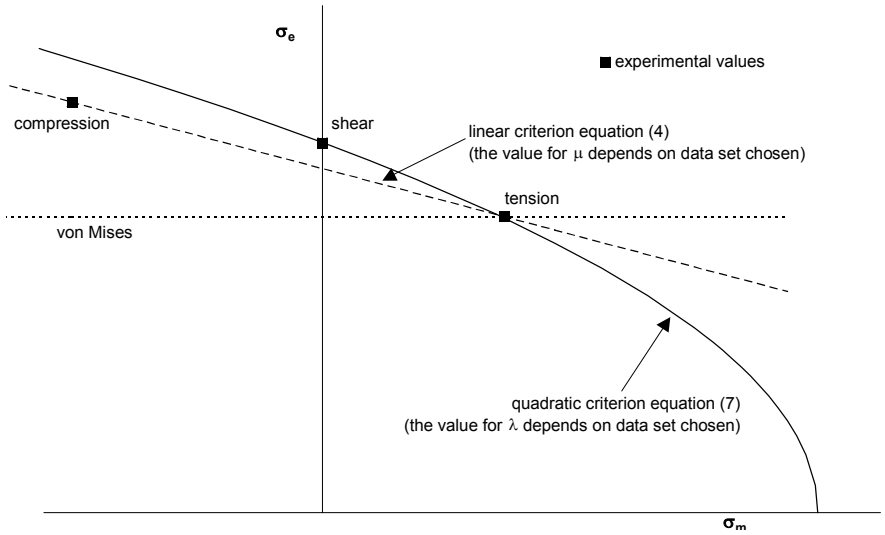

Figure 3: Plot of equivalent stresses under tension, shear and compression at an effective plastic strain of 0.03 on axes of effective shear stress σ_e against hydrostatic stress σ_m.

If the materials models described above are used to analyse data from uniaxial compression, tension and shear, some limitations of the models are revealed. Figure 2 compares experimental data for true yield stress against true plastic strain measured on a rubber-toughened adhesive. When compared with the curve derived from a shear test, the data under compression and tension reveal a dependence of yielding on the hydrostatic component of stress. This is typical for this type of material and demonstrates that the von Mises criterion is inaccurate. The hydrostatic-stress-sensitivity parameters μ and λ can be determined from data measured under two different states of stress. The derived values for these parameters, however, depend upon which test data are selected. This is illustrated in Figure 3, which shows measured yield stresses obtained from the curves in Figure 2 and plotted on axes of deviatoric stress σ_e against hydrostatic stress σ_m (see Equations (2) and (6)). The yield stresses were determined at an effective plastic strain of 0.03. Figure 3 allows direct comparison of experimental data with the yield criteria in Equations (3), (4) and (7).

The inadequacy of the von Mises criterion is immediately apparent. The parameter μ in the linear Drucker-Prager criterion is the gradient of the line joining two data points, and this gradient is seen to be dependent on the data pair selected. Similarly, the value for the parameter λ derived for the quadratic criterion (exponent Drucker-Prager) also depends on the data set selected. These inconsistencies between measured and predicted behaviour for the rubber-toughened epoxy can be explained by the nucleation of cavities in the rubber phase. The nucleation of cavities requires a dilatational stress component and does not therefore occur under shear or compression. Its effect is to lower the tensile yield stress relative to the shear or compression stresses. Furthermore, cavitation creates the additional volumetric strain under tension which gives rise to a decrease in Poisson's ratio with plastic strain observed for this type of material and illustrated in Figure 4.

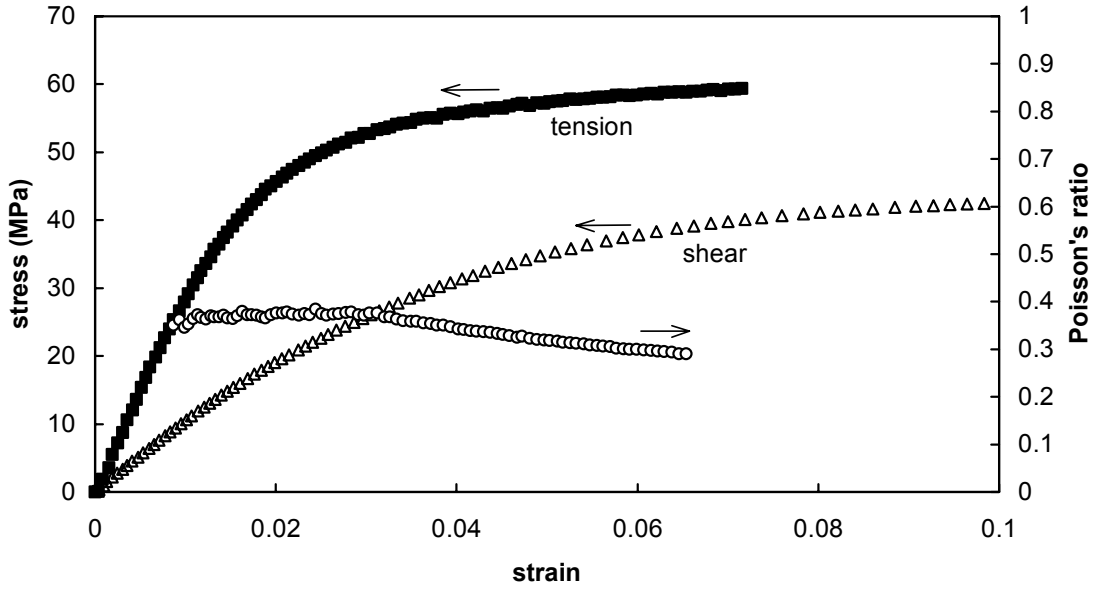

Figure 4: Stress/strain curves and Poisson's ratio for a rubber-toughened epoxy adhesive in tension and shear at the same effective plastic strain rate of 0.002s^{-1}.

Attempts have been made to include the influence of void nucleation on ductility through adaptations to elastic-plastic models [1]. The yield criterion in Equation (4) is modified as follows to give a yield potential Φ that includes the effect of cavitation of the rubber on yield stresses:

$$\Phi = \frac{\sigma_e^2}{\sigma_M^2} - (q_1 f)^2 + 2q_1 f \cosh \frac{3\sigma_m}{2\sigma_M} - \left(1 - \frac{\mu\sigma_m}{\sigma_M}\right)^2 = 0 \qquad (8)$$

where $\mathbf{f}$ is the effective volume fraction of cavities, which at small strains is zero, but increases rapidly over some characteristic strain region responsible for cavity nucleation. The parameter $\mathbf{q_1}$ was proposed to account for the effect of void interactions on the stress distribution in the matrix between cavities. The yield stress $\boldsymbol{\sigma_M}$ is $\sqrt{3}$ × the shear yield stress for the matrix material between voids. It is assumed that a cavity is nucleated in a rubber particle at some critical volumetric strain that decreases with increasing particle diameter. For a distribution of particle sizes, the void nucleation should then occur over a range of total volumetric strain $\boldsymbol{\varepsilon_v}$ related to the critical volumetric strain range for the rubber particles.

Various mathematical functions relating **f** and ε_v have been considered and, based on tensile and shear results for the rubber-toughened adhesive and some rubber-toughened thermoplastics, the most suitable takes the form:

$$f = 0 \quad \text{for } \varepsilon_v \le \varepsilon_{1v} \tag{9}$$

$$f = v_{Ro}\left\{1-\exp\left[-\left(\frac{\varepsilon_v-\varepsilon_{1v}}{\varepsilon_{2v}}\right)^{\beta}\right]\right\} \quad \text{for } \varepsilon_v > \varepsilon_{1v} \tag{10}$$

These expressions imply that cavities start to nucleate when the volumetric strain exceeds a critical value ε_{1v} after which the volume fraction **f** rises from zero to the value v_{Ro}, the total volume fraction of rubber, over a range of volumetric strain determined by the parameters ε_{2v} and β. Furthermore, for stress states such as compression and shear that do not generate a significant volumetric strain, **f = 0** and Equation (8) is identical to Equation (4).

2.5 A COMPARISON OF ELASTIC-PLASTIC MODEL PREDICTIONS

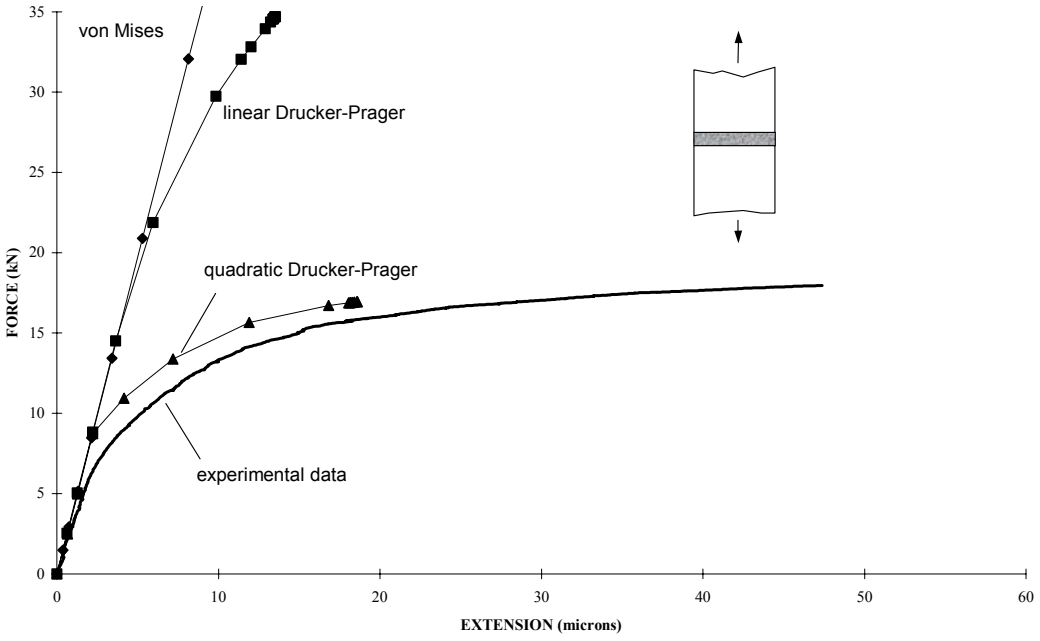

Figure 5: Comparison of the force against extension for a butt-joint specimen with predictions made using three different models available in ABAQUS.

To demonstrate some limitations in the predictive accuracy of the elastic-plastic models described in this report, predicted axial stress against axial strain curves for a butt-joint specimen loaded in tension are compared with experimental data in Figure 5. The adhesive is the rubber-toughened epoxy referred to earlier. The joint thickness is 0.5 mm and its diameter is 25 mm. Because of the large diameter-to-thickness ratio of the adhesive layer, the strain distribution is predominantly pure uniaxial. This results from lateral stresses that are imposed by the adherends in the plane of the adhesive layer that prevent lateral contraction under the applied axial force. The stress and strain states generated in the adhesive are similar to those produced in regions of many joints where the peel stress is high and failure usually initiates.

Of the predicted curves, the exponent Drucker-Prager and the cavitation models give satisfactory agreement with data. The former model predicts lateral stresses that increase during plastic deformation to the value of the axial stress (implying pure hydrostatic tension). The cavitation model predicts lateral stresses that increase to only about half the axial value. Because the cavitation model attempts to describe a realistic plastic deformation mechanism in the adhesive, this model should give the more accurate predictions of stress and strain in regions of high peel stress. Use of the cavitation model should therefore aid the development of a valid failure criterion in the latter stages of Project MMS11.

3. MODELLING NON-LINEAR CREEP DEFORMATION OF POLYMERS

3.1 A CREEP MODEL FOR GLASSY POLYMERS

Relaxation processes in which time-dependent changes in the conformation of polymer molecules are produced in response to an applied stress σ_o cause creep in glassy polymers. The resulting creep deformation of the material is characterised by a time-dependent strain $\varepsilon(t)$ from which a creep compliance function is derived [2]:

$$D(t) = \varepsilon(t)/\sigma_o \tag{11}$$

A number of mathematical functions have been used to model experimental results. The function, shown below, has been used successfully at temperatures well below the glass transition temperature:

$$D(t) = D_o \exp(t/\tau)^n \tag{12}$$

The parameter τ is identified with a mean retardation time for the creep process, which has a distribution of retardation times related to the magnitude of the parameter **n**. $\mathbf{D_o}$ is the elastic compliance and is equal to the inverse of the Young's modulus measured at an appropriate strain rate.

Since the parameter τ in Equation (12) is assumed to be constant, the equation does not take account of physical ageing in the material. Physical ageing is associated with a slow reorganisation of the structure of the polymer following cooling from its processing temperature. These changes reduce the molecular mobility over a long period of time, which, under creep loading, gives rise to a progressive increase in the parameter τ with creep time. This produces a shift in the creep function at large creep times, which can be modelled [3] if the age and ageing rate of the material are known.

For small creep stresses, τ is independent of the stress magnitude and the creep behaviour is linear. At higher stresses, creep curves are observed to shift to shorter times as shown in Figure 6 for experimental data obtained on PVC. This shift is interpreted as an increase in molecular mobility brought about by the application of elevated stresses that results in a reduction in the mean retardation time τ. It is this enhanced mobility that gives rise to non-linear creep behaviour. The increase in mobility is short lived and, subsequent to load application, τ increases relatively quickly with time under load analogous to enhanced physical ageing. Modelling the stress and time dependences of τ and how they influence the creep deformation is still a subject for further research.

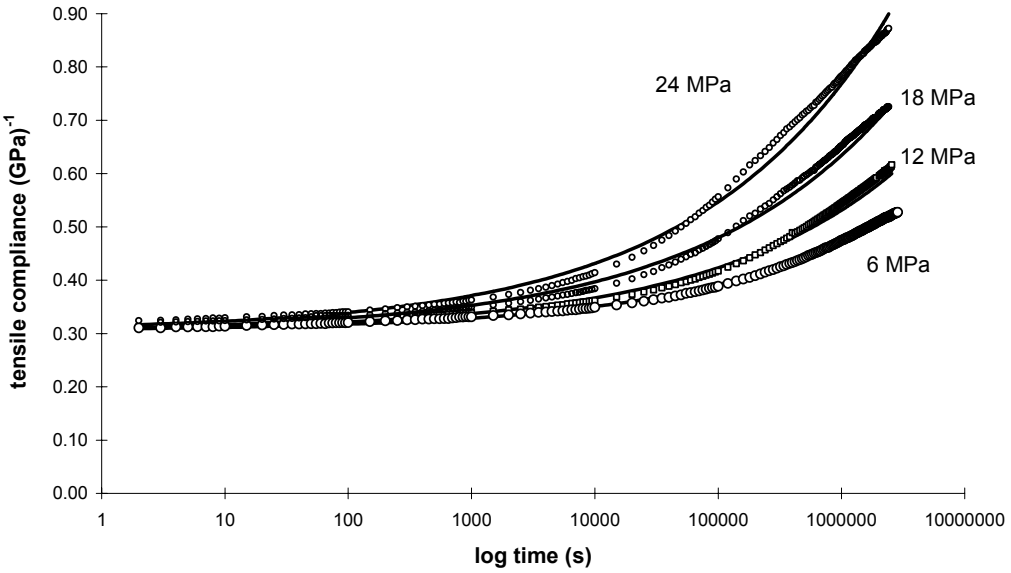

Figure 6: Tensile creep compliance curves for PVC at different levels of stress. Creep behaviour is modelled using Equations (13) and (14) in which the effects of physical ageing have been neglected.

For the application considered here, the effects of physical ageing on the creep compliance will be neglected. For this situation, a simple power law can adequately model the creep data in Figure 6 as follows:

$$D(t) = D_o\ (1 + t/\tau)^n \tag{13}$$

Values for the parameters $\mathbf{D_o}$, $\boldsymbol{\tau}$ and **n** have been chosen to give the optimum fit to the experimental data. The fits are shown in Figure 6. The values for $\mathbf{D_o}$ and **n** are the same for each curve. The parameter $\boldsymbol{\tau}$ is different for each stress level but is assumed constant with creep time. This neglect of any variation of $\boldsymbol{\tau}$ with creep time through physical ageing is responsible for the inability of Equations (12) or (13) to accurately describe the shape of the experimental results. The dependence of $\boldsymbol{\tau}$ on stress is adequately described by the following relationship, which is based on the Eyring equation for molecular transitions across a potential barrier whose height is changed by the applied stress.

$$\tau = \frac{A\sigma}{\sinh(a\,\sigma)} \tag{14}$$

where **a** and **A** are material parameters. Values for the parameters in Equations (13) and (14) that were used to obtain the fits to the data in Figure 6 are shown in Table 1.

Table 1: Parameter Values in Equations (13) and (14) used to model creep in PVC

$\mathbf{D_o}$ ($\mathbf{GPa^{-1}}$)	**n**	**A** ($\mathbf{s.MPa^{-1}}$)	**a** ($\mathbf{MPa^{-1}}$)
0.305	0.28	4.2×10^6	0.3

Equations (13) and (14) describe creep under a uniaxial tensile stress. However, Equation (13) can be generalised to apply to multiaxial creep stress states as follows:

$$\varepsilon_{ij}(t)=\left((1+\nu)\,D_o\,\sigma_{ij}-3\nu\,D_o\,\sigma_m\,\delta_{ij}\right)(1+(t/\tau)^n) \tag{15}$$

$$\tau=\frac{A\bar{\sigma}}{\sinh(a\bar{\sigma})} \tag{16}$$

The parameter $\bar{\sigma}$ is an effective stress and accounts for the observation that the reduction of τ with stress depends on the stress state as well as the stress magnitude. This is demonstrated through an analysis of creep tests under uniaxial compression where the reduction of τ for a given stress level is observed to be significantly less than that obtained under the same uniaxial tensile stress. This suggests that it is the shear component of stress ($\boldsymbol{\sigma_e}$ in Equation (2)) that is mainly responsible for reducing $\boldsymbol{\tau}$, but this reduction is also influenced by the hydrostatic component $\boldsymbol{\sigma_m}$ (see Equation (6)), such that $\boldsymbol{\tau}$ is decreased more in tension, where $\boldsymbol{\sigma_m}$ is positive, than it is in compression where $\boldsymbol{\sigma_m}$ is negative.

By analogy with the influence of hydrostatic stress on yielding in plastics (Equation (4)), an expression for $\bar{\sigma}$ of the following form has been considered:

$$\bar{\sigma} = \sigma_e + \bar{\mu}\,\sigma_m \tag{17}$$

From analyses of non-linear creep data for PVC under tension and compression, a value for $\boldsymbol{\bar{\mu} = 1}$ was derived.

3.2 APPLICATION OF THE MODEL USING FINITE ELEMENT ANALYSIS

The creep function given by Equation (15) with Equation (16) treats creep as time-dependent elasticity. Since the time dependent term is also influenced by the stress magnitude, then non-linear behaviour is modelled. Non-linear creep in FEA packages is generally modelled by time-dependent plasticity. These models are widely applicable to creep in metallic materials but require some evaluation before they can be used to represent the behaviour observed with plastics and described by Equation (15). This is considered next.

In time-dependent plasticity models, the total strain is the sum of elastic and plastic components with the plastic strain component being responsible for time-dependence, and hence creep deformation. An expression for the creep strain rate is derived from the flow law and in ABAQUS takes the form:

$$\dot{\varepsilon}_{ij} = \dot{\varepsilon}_s\,\frac{3\sigma_{ij}}{2\sigma_e}+\left(\dot{\varepsilon}_{sw}-\frac{3\sigma_m}{2\sigma_e}\,\dot{\varepsilon}_s\right)\delta_{ij} \tag{18}$$

Here $\boldsymbol{\dot{\varepsilon}_s}$ and $\boldsymbol{\dot{\varepsilon}_{sw}}$ are considered as contributions to the strain rate arising from shear and volumetric (swelling) deformation mechanisms.

Differentiating the creep strain, Equation (15), given by the model for creep in plastics gives the following expression for the strain rate, which is analogous to Equation (18)

$$\dot{\varepsilon}_{ij}(t) = \frac{n}{\tau^n}\left[(1+\nu) D_o \sigma_{ij} - 3\nu D_o \sigma_m \delta_{ij}\right] t^{n-1} \qquad (19)$$

assuming the Poisson's ratio ν is independent of time. This can be identified with Equation (18) if:

$$\dot{\varepsilon}_s = \frac{2\sigma_e}{3} \frac{n}{\tau^n} (1+\nu)\, D_o\, t^{n-1} \qquad (20)$$

and

$$\dot{\varepsilon}_{sw} = \frac{n\sigma_m}{\tau^n} (1+2\nu)\, D_o\, t^{n-1} \qquad (21)$$

Thus $\dot{\varepsilon}_s$ and $\dot{\varepsilon}_{sw}$ in the time-dependent plasticity model can be determined from a knowledge of materials parameters n, τ, ν and D_o, and the creep stress state identified by σ_e and σ_m.

Use of this model in a stress analysis of an adhesively bonded joint would reveal a redistribution of stress and strain levels through the bond with time when under load resulting from non-linear creep in the adhesive.

4. PREDICTION OF FAILURE IN ADHESIVES

4.1 MONOTONIC LOADING

Failure of a bonded joint usually occurs by the initiation and growth of a crack in the adhesive layer. Depending on the properties of the adhesive, the joint geometry and the load history, the growth phase can be rapid after crack initiation or slow until a critical length is reached for rapid fracture. Failure initiation can either be by rupture of the adhesive (cohesive failure) or by loss of adhesion with an adherend (adhesion failure). Failure will initiate in a region of high stress or strain and, since these regions often arise at the interface with the adherend, it can be difficult to diagnose whether the failure is by loss of cohesion or adhesion. Different failure criteria will presumably apply to each of these processes.

Studies that aim to identify a failure criterion for a particular adhesive use stress analysis to determine stress and strain distributions in the adhesive layer and seek to identify a critical component and level for failure that is independent of the joint dimensions and applies to different joint geometries. This work is made complicated by the fact that regions of peak stress and strain can be highly localised and therefore dependent on the mesh size. Calculations are also sensitive to the precise geometry of the ends of the adherends and the shape of the fillets on the adhesive layer. Ideally, singularities in the analysis arising from sharp edges and corners should be avoided. Furthermore, the stress and strain states in the regions of peak stress and strain usually contain high hydrostatic components. As indicated in Section 2.5, the accuracy of stress and strain predictions under these conditions using available materials models is uncertain and results may have significant errors. This hinders the identification of a realistic and widely applicable criterion. Several criteria that have been proposed in various failure studies are listed in Table 2 [4-14].

Table 2: Proposed Failure Criteria in Different Studies on Adhesive Joints

Based on a critical quantity at a point
• Peel stress • Maximum principal stress • Maximum strain • Plastic energy density
Based on a critical value at a distance from a singularity
• Peel stress • Maximum principal stress

Any criterion based on a critical level of stress is likely to be conservative for toughened adhesives since it is clear from results such as those given in Figures 1 and 5, that these materials are able to sustain further deformation by plastic flow after the maximum stress is reached. An exception to this statement may apply to a criterion based on the maximum peel or hydrostatic stress since the scope for extensive plastic deformation under these stress states is limited even in toughened adhesives.

Criteria based on a critical level of stress or strain at a distance have been proposed to overcome the problem of stress or strain singularities, but have met with limited success because the critical distance is not a material property but depends on factors such as the joint geometry, the bond layer thickness and the mode of loading.

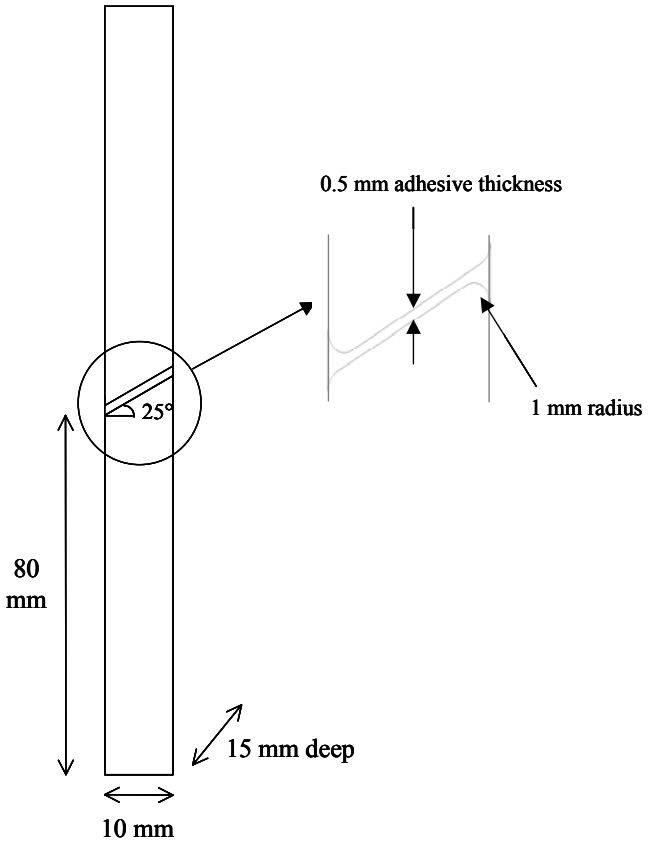

Figure 7: Schematic diagram of the scarf-joint specimen showing the dimensions and the geometry of the adherends.

The choice of a strain-based criterion is limited by the following consideration. Tests on adhesives involving butt-joint specimens under torsion generally exhibit large strains at failure, even for adhesives showing relatively low failure strains when tested under uniaxial tension using bulk specimens. This indicates that adhesives are tolerant of shear strains and that failure in other shear tests, such as the thick adherend and the lap shear tests is controlled by local peel rather than shear strains. This means that even the maximum principal strain criterion is unlikely to be valid (this is high under pure shear) unless there is a significant hydrostatic strain contributing to the principal strain. Based on these considerations, a criterion based on a critical hydrostatic strain, or a combination of hydrostatic and shear (deviatoric) components achieving a critical net value, may be a realistic proposal for further study.

Future studies aimed at identifying a valid failure criterion will benefit from the use of more realistic materials models for use with a FE system to predict stress and strain values at the site of crack initiation. The model that takes account of cavitation in rubber particles outlined in Section 2.4 was developed for this purpose. Even with the use of better materials models, some caution may be needed in the interpretation of predictions of stress and strain levels when peak values are highly localised. Strain localisation is observed (and predicted) during plastic deformation because of the decrease in the stiffness of the material with increases in strain. Under these circumstances, there is some uncertainty in the accuracy with which an FE analysis can predict the magnitude of stress and strain levels in regions that are highly localised.

To illustrate some of the uncertainties associated with available models, stress and strain distributions have been calculated in the adhesive layer in the scarf joint shown in Figure 7. The joint failed at an extension of 0.035 mm. The distributions of the maximum principal stress and the maximum principal strain at this extension are shown in Figures A1.1 and A1.2 of Appendix 1 using the von Mises, the linear Drucker-Prager and the exponent Drucker-Prager materials models described in Sections 2.1, 2.2 and 2.3 in this report. The stress and strain distributions predicted by the two Drucker-Prager models differ in both the magnitude and location of peak values. Studies of crack initiation therefore benefit from simultaneous observations that locate the point at which the crack initiates in the adhesive. In the scarf joint illustrated here, failure was too rapid to locate the region of initiation, but the lap joint showed some slow crack growth prior to rapid fracture.

4.2 CREEP AND FATIGUE LOADING

Studies of crack initiation under creep or fatigue loading will initially explore the possibility of using failure criteria that have proved suitable for monotonic loading. If a critical local stress or strain level at failure proves to be successful, then it seems likely that critical values will be time-dependent in the case of creep loading and cycle-number and stress-ratio dependent in the case of fatigue loading. If the crack initiates at the same location under creep and fatigue as it does under monotonic loading, then this would support exploration of the same formulation for the criterion under these load histories. Under long-term loading conditions, a redistribution of stress and strain will occur in some regions of the adhesive through non-linear creep and stress relaxation. This redistribution will be different in different joint geometries and may need to be taken into account when determining critical properties for the criterion.

5. MODELLING ANISOTROPIC ELASTICITY OF LAMINATES

Analysis of composite materials can be considered in degrees of structural complexity building up from micromechanics scale (i.e. ply or lamina level) to the formation of laminates from the properties, fibre orientation and distribution of individual laminae (i.e. macromechanics scale). This section of the report examines the three-dimensional (3-D) analysis required for characterising the stress-strain behaviour of composites under uniaxial and multiaxial loading conditions. Laminate theory is briefly described along with comments on underlying assumptions [15-16].

5.1 UNIDIRECTIONAL LAMINATES

In order to analyse a multidirectional 3-D laminate, it is necessary to initially examine the elastic behaviour of a single unidirectional lamina. From this initial point, a logical progression can be made to the prediction of macromechanical behaviour of a laminate. Although, the properties of a lamina on a microscopic scale are inherently heterogeneous and variable from point to point, on a macroscopic scale the lamina may be considered as a homogeneous anisotropic layer. The lamina properties are uniform in any given direction and are dependent on the properties of the lamina constituents. Behaviour of the constituents is considered to be linear-elastic to failure. Constituents are also considered to be homogeneous and isotropic. Furthermore, the analysis assumes that there are no defects (e.g. voids) present within the composite structure and there is perfect interfacial bonding between fibre and matrix.

In general, the state of stress at a point in a body can be described by the nine components of the stress tensor $\boldsymbol{\sigma_{ij}}$. Correspondingly, the strain tensor $\boldsymbol{\varepsilon_{ij}}$ also has nine components. The linear relationship between stress and strain can be expressed as:

$$\sigma_{ij} = E_{ijkl}\varepsilon_{ij} \tag{22}$$

The components of the fourth-order tensor $\mathbf{E_{ijkl}}$ are known as the stiffness tensor (i.e. elastic constants). The stress-strain relation given in Equation (22) can be expressed in the inverted form as:

$$\varepsilon_{ij} = C_{ijkl}\sigma_{ij} \tag{23}$$

where $\mathbf{C_{ijkl}}$ is known as the compliance tensor. For orthotropic unidirectional lamina, the 81 components of the fourth-order tensor $\mathbf{C_{ijkl}}$ reduce to 36 of which only 21 components are independent. The relationships given by Equations (22) and (23) reduce to the following form:

$$\sigma_{ij} = Q_{ij}\varepsilon_{ij} \tag{24}$$

and

$$\varepsilon_{ij} = C_{ij}\sigma_{ij} \tag{25}$$

where $\boldsymbol{\sigma_{ij}}$ are the stress components, $\boldsymbol{\varepsilon_{ij}}$ the strain components, $\mathbf{Q_{ij}}$ is the stiffness matrix and $\mathbf{C_{ij}}$ is the compliance (i.e. inverse stiffness matrix).

The expanded stress-strain relationship given by Equation (25) for an orthotropic unidirectional lamina is shown below.

$$\begin{Bmatrix}\varepsilon_{11}\\ \varepsilon_{22}\\ \varepsilon_{33}\\ \gamma_{23}\\ \gamma_{31}\\ \gamma_{12}\end{Bmatrix}=\begin{bmatrix}C_{11} & C_{12} & C_{13} & 0 & 0 & 0\\ C_{12} & C_{22} & C_{33} & 0 & 0 & 0\\ C_{13} & C_{23} & C_{33} & 0 & 0 & 0\\ 0 & 0 & 0 & C_{44} & 0 & 0\\ 0 & 0 & 0 & 0 & C_{55} & 0\\ 0 & 0 & 0 & 0 & 0 & C_{66}\end{bmatrix}\begin{Bmatrix}\sigma_{11}\\ \sigma_{22}\\ \sigma_{33}\\ \tau_{23}\\ \tau_{31}\\ \tau_{12}\end{Bmatrix} \tag{26}$$

The above relationship can be rewritten in terms of nine independent elastic material constants $\mathbf{E_{11}}$, $\mathbf{E_{22}}$, $\mathbf{E_{33}}$, $\mathbf{G_{12}}$, $\mathbf{G_{13}}$, $\mathbf{G_{23}}$, $\boldsymbol{\nu_{12}}$, $\boldsymbol{\nu_{13}}$ and $\boldsymbol{\nu_{23}}$ as follows:

$$\begin{Bmatrix}\varepsilon_{11}\\ \varepsilon_{22}\\ \varepsilon_{33}\\ \gamma_{23}\\ \gamma_{31}\\ \gamma_{12}\end{Bmatrix}=\begin{bmatrix}\frac{1}{E_{11}} & -\frac{\nu_{21}}{E_{22}} & -\frac{\nu_{31}}{E_{33}} & 0 & 0 & 0\\ -\frac{\nu_{12}}{E_{11}} & \frac{1}{E_{22}} & -\frac{\nu_{32}}{E_{33}} & 0 & 0 & 0\\ -\frac{\nu_{13}}{E_{11}} & -\frac{\nu_{23}}{E_{22}} & \frac{1}{E_{33}} & 0 & 0 & 0\\ 0 & 0 & 0 & \frac{1}{G_{23}} & 0 & 0\\ 0 & 0 & 0 & 0 & \frac{1}{G_{31}} & 0\\ 0 & 0 & 0 & 0 & 0 & \frac{1}{G_{12}}\end{bmatrix}\begin{Bmatrix}\sigma_{11}\\ \sigma_{22}\\ \sigma_{33}\\ \tau_{23}\\ \tau_{31}\\ \tau_{12}\end{Bmatrix} \tag{27}$$

For orthotropic materials, the following reciprocal relationships must be satisfied:

$$\frac{\nu_{12}}{E_{11}}=\frac{\nu_{21}}{E_{22}},\quad \frac{\nu_{13}}{E_{11}}=\frac{\nu_{31}}{E_{33}},\quad \frac{\nu_{23}}{E_{22}}=\frac{\nu_{32}}{E_{33}} \tag{28}$$

5.2 ORIENTED ORTHOTROPIC LAMINATES

For oriented balanced and symmetric laminates loaded in the **x-**, **y-** or **z-**direction, the stress-strain relationship is as follows:

$$\begin{Bmatrix}\varepsilon_{11}\\ \varepsilon_{22}\\ \varepsilon_{33}\\ \gamma_{23}\\ \gamma_{31}\\ \gamma_{12}\end{Bmatrix}=\begin{bmatrix}\bar{C}_{11} & \bar{C}_{12} & \bar{C}_{13} & 0 & 0 & 0\\ \bar{C}_{12} & \bar{C}_{22} & \bar{C}_{23} & 0 & 0 & 0\\ \bar{C}_{13} & \bar{C}_{23} & \bar{C}_{33} & 0 & 0 & 0\\ 0 & 0 & 0 & \bar{C}_{44} & 0 & 0\\ 0 & 0 & 0 & 0 & \bar{C}_{55} & 0\\ 0 & 0 & 0 & 0 & 0 & \bar{C}_{66}\end{bmatrix}\begin{Bmatrix}\sigma_{11}\\ \sigma_{22}\\ \sigma_{33}\\ \tau_{23}\\ \tau_{31}\\ \tau_{12}\end{Bmatrix} \tag{29}$$

The stress-strain relationship can be rewritten in terms of the effective engineering elastic constants $\mathbf{E_{xx}}$, $\mathbf{E_{yy}}$, $\mathbf{E_{zz}}$, $\mathbf{G_{xy}}$, $\mathbf{G_{xz}}$, $\mathbf{G_{yz}}$, $\boldsymbol{\nu}_{\mathbf{xy}}$, $\boldsymbol{\nu}_{\mathbf{xz}}$ and $\boldsymbol{\nu}_{\mathbf{yz}}$ as follows.

$$\begin{Bmatrix} \varepsilon_{xx} \\ \varepsilon_{yy} \\ \varepsilon_{zz} \\ \gamma_{yz} \\ \gamma_{zx} \\ \gamma_{xy} \end{Bmatrix} = \begin{bmatrix} \frac{1}{E_{xx}} & -\frac{\nu_{yx}}{E_{yy}} & -\frac{\nu_{zx}}{E_{zz}} & 0 & 0 & 0 \\ -\frac{\nu_{xy}}{E_{xx}} & \frac{1}{E_{yy}} & -\frac{\nu_{zy}}{E_{zz}} & 0 & 0 & 0 \\ -\frac{\nu_{xz}}{E_{xx}} & -\frac{\nu_{yz}}{E_{yy}} & \frac{1}{E_{zz}} & 0 & 0 & 0 \\ 0 & 0 & 0 & \frac{1}{G_{yz}} & 0 & 0 \\ 0 & 0 & 0 & 0 & \frac{1}{G_{zx}} & 0 \\ 0 & 0 & 0 & 0 & 0 & \frac{1}{G_{xy}} \end{bmatrix} \begin{Bmatrix} \sigma_{xx} \\ \sigma_{yy} \\ \sigma_{zz} \\ \tau_{yz} \\ \tau_{zx} \\ \tau_{xy} \end{Bmatrix} \tag{30}$$

The following reciprocal relationships must be satisfied.

$$\frac{\nu_{xy}}{E_{xx}} = \frac{\nu_{yx}}{E_{yy}}, \quad \frac{\nu_{xz}}{E_{xx}} = \frac{\nu_{zx}}{E_{zz}}, \quad \frac{\nu_{yz}}{E_{yy}} = \frac{\nu_{zy}}{E_{zz}} \tag{31}$$

5.3 DISCUSSION

The above analysis applies to balanced and symmetric laminates. For unbalanced and asymmetric laminates, the analysis is modified to include coefficients of mutual influence and Chentsov's coefficients (for further details see [17]). Although the analysis does not account for non-linear material behaviour, or thermal and moisture effects, it can be readily modified to account for hygrothermal induced stresses and strains [16]. The nine independent elastic properties $\mathbf{E_{11}}$, $\mathbf{E_{22}}$, $\mathbf{E_{33}}$, $\mathbf{G_{12}}$, $\mathbf{G_{13}}$, $\mathbf{G_{23}}$, $\boldsymbol{\nu}_{\mathbf{12}}$, $\boldsymbol{\nu}_{\mathbf{13}}$ and $\boldsymbol{\nu}_{\mathbf{23}}$ can be determined experimentally or calculated using micromechanics formulations, such as those used in CoDA (Composite Design and Analysis) preliminary design software, developed by the NPL.

6. MODELS FOR PREDICTING COMPOSITE LAMINATE FAILURE

This section examines physics/mechanistic, fracture mechanics and non-mechanistic (i.e. statistical and empirical) based models that can be used to predict laminate failure under monotonic, creep and fatigue loading conditions.

6.1 MONOTONIC LOADING

6.1.1 Classical Laminate Analysis

An approach commonly used for determining degradation of multi-directional laminates is to use classical laminate failure analysis (e.g. Hill's and Tsai-Wu failure criterion) with de-rated lamina elastic and strength properties. The lamina data can either be measured or determined using micromechanics equations (e.g. rule of mixtures and Tsai-Halpin).

Hills's failure criterion or maximum work theory, developed for anisotropic materials (i.e. composites), is based on von Mises yield criterion for a homogeneous and isotropic solid. Assuming plane stress conditions, Hill's failure criterion can be written as [18]:

$$\left(\frac{\sigma_{11}}{S_{11}}\right)^2+\left(\frac{\sigma_{22}}{S_{22}}\right)^2+\left(\frac{\tau_{12}}{S_{12}}\right)^2=1 \tag{32}$$

where σ_{11}, σ_{22} and τ_{12} are the in-plane longitudinal, transverse and shear stresses, and S_{11}, S_{22} and S_{12} are the corresponding strengths in the principal material directions. In many cases, σ_{33} will not be negligible. The failure criterion describes an ellipsoid failure criterion.

Azzi and Tsai [19] modified Hill's anisotropic yield criterion to account for the interaction between failure modes in composite materials. The modified equation, known as the Tsai-Hill failure criterion, is given below:

$$\left(\frac{\sigma_{11}}{S_{11}}\right)^2-\frac{\sigma_{11}\sigma_{22}}{S_{11}^2}+\left(\frac{\sigma_{22}}{S_{22}}\right)^2+\left(\frac{\tau_{12}}{S_{12}}\right)^2=1 \tag{33}$$

Tsai and Wu [20] proposed the following stress-formulated failure criterion for orthotropic lamina subjected to plane stress:

$$F_1\sigma_{11}+F_2\sigma_{22}+F_{11}\sigma_{11}^2+F_{22}\sigma_{22}^2+F_{66}\tau_{12}^2+2F_{12}\sigma_{11}\sigma_{22}\geq 1 \tag{34}$$

where F_1, F_2, F_{11}, F_{22} and F_{66} are strength coefficients.

Strength coefficients in Equation (34) are expressed in terms of the longitudinal tensile strength $S_{11}(T)$, transverse tensile strength $S_{22}(T)$, longitudinal compressive strength $S_{11}(C)$, transverse compressive strength $S_{22}(C)$ and shear strength S_{12} as follows [20]:

$$F_1=\frac{S_{11}(C)-S_{11}(T)}{S_{11}(T)\,S_{11}(C)} \qquad F_2=\frac{S_{22}(C)-S_{22}(T)}{S_{22}(T)\,S_{22}(C)}$$
$$F_{11}=\frac{1}{S_{11}(T)\,S_{11}(C)} \qquad F_{22}=\frac{1}{S_{22}(T)\,S_{22}(C)} \qquad F_{66}=\frac{1}{S_{12}^2} \tag{35}$$

The interaction term F_{12} in Equation (34) is determined by the following relationship [20-21]:

$$F_{12}=-\frac{\sqrt{(F_{11}F_{22})}}{2} \tag{36}$$

It is important to realise that the Tsai-Wu failure theory does not provide information on fracture mechanisms account for interfacial effects and is not directly translatable to laminated structures. Despite this, most current laminate analysis software packages contain both the Tsai-Hill and the Tsai-Wu failure criteria. Both failure criteria ignore the microstructure where failure mechanisms operate and are unable to account for sub-critical events leading to final failure. Failure analysis can be considered essentially a curve fitting exercise with many authors concurring that the Tsai-Wu tensor failure theory provides better agreement with experimental data than the other failure criteria in use today.

6.1.2 Weakest Link Failure Hypothesis

This approach assumes that a structure consists of an assembly of small elements in which the stress state is more or less uniform [22]. The strength of these elements is a random variable. For fibrous materials, the elements align in series along the length of the fibres (forming a chain). The chain breaks in tension when one or more of the links fail. The failure event is controlled by the weakest link (or links) in the chain. Most subsequent statistical treatments of failure adhere strictly to this hypothesis.

Suppose that **F(s)** is the cumulative strength distribution for one element of the system (i.e. **F(s)** is the probability that the strength of the element is less than **s**). The quantity **1 - F(s)** is, therefore, the probability that the strength of the element is greater than σ. For an assembly of **N** elements arranged as a chain (as would be the case for a fibre), each with statistically independent strength characteristics and each subjected to a uniform stress **s**, the probability that the assembly survives is $[1 - F(s)]^N$ since each element must have strength greater than σ. The probability that the application of the stress **s** causes the failure of at least one element is then given by:

$$P_f(\sigma) = 1 - [1 - F(\sigma)]^N \tag{37}$$

Equation (37) is a mathematical statement of the weakest link failure hypothesis and is only valid for structures where the number of elements **N** is large ($N \to \infty$). It has therefore been necessary to derive an asymptotic form of the weakest link model (asymptotic theory of extreme values). The strength of brittle solids can be described by the Weibull strength distribution [22]:

$$P_f(\sigma) = 1 - \exp\left[- N\left(\frac{\sigma - \sigma_0}{\sigma_c} \right)^m \right], \sigma_c > 0, m > 0, \sigma \geq \sigma_0, \quad P_f(\sigma) = 0 \quad \text{if} \quad \sigma < \sigma_0 \tag{38}$$

where σ_0 is the lower strength limit, σ_c is the difference between the upper strength limit σ_U and the lower strength limit σ_0 ($\sigma_U - \sigma_0$) and **m** is an experimental measure of scatter in strength. The Weibull strength distribution is the probability of failure occurring at a stress level equal to or less than σ.

A volumetric form of Equation (37) is shown below [22]:

$$P_f(\sigma, V) = 1 - \exp\left[- \frac{V}{V_0}\left(\frac{\sigma - \sigma_0}{\sigma_c} \right)^m \right], \sigma \geq \sigma_0 \tag{39}$$

where the total volume $V = NV_0$ (sum of all the volume elements). The above relationship indicates that failure probability is dependent upon component size. Also, the failure probability function approaches a value of 1 for $\sigma > \sigma_0$ when $V \to \infty$. The following relationship can be used in most engineering applications for representing the distribution of strength data [22]:

$$f(\sigma) = \left(\frac{\sigma - \sigma_0}{\sigma_c} \right), \quad \text{if } \sigma \geq \sigma_0, \text{ otherwise } f(\sigma) = 0 \tag{40}$$

6.1.3 Fracture Mechanics

A major consideration in the design of composite and bonded structures is the possibility of crack growth. Crack growth can be catastrophic when the strain-energy release rate **G** of the system has been exceeded. Delaminations or debonds (i.e. planar cracks) are probably the most life-limiting defects that occur in layered or laminated structures, and may arise during processing or subsequent service. Common structural features, such as thickness changes, bolted holes or bonded joints, generate through-thickness stress concentrations, which may initiate delaminations under static or cyclic loading conditions.

Crack initiation and growth usually occurs under mixed mode conditions, a combination of:

- Mode I (crack opening)
- Mode II (forward shear)
- Mode III (scissor shear)

In most practical applications, composite and bonded structures experience mixed-mode loading conditions involving $\mathbf{G_I}$ and $\mathbf{G_{II}}$ (and in some cases $\mathbf{G_{III}}$) due to the presence of peel and in-plane shear stresses, resulting in mixed-mode cracking. The total strain-energy release-rate $\mathbf{G_T}$ (or $\mathbf{G_c}$) is often represented by either a linear interaction or a quadratic relationship [23-24]:

$$\frac{G_I}{G_{Ic}} + \frac{G_{II}}{G_{IIc}} = 1 \tag{41}$$

$$\left(\frac{G_I}{G_{Ic}}\right)^2 + \left(\frac{G_{II}}{G_{IIc}}\right)^2 = 1 \tag{42}$$

where $\mathbf{G_{Ic}}$ and $\mathbf{G_{IIc}}$ are the mode I and mode II critical strain release rates, respectively.

Experimental evidence from mixed-mode I/II fracture (MMF) tests tends to support a quadratic relationship. The double cantilever beam (DCB) test is often used for measuring $\mathbf{G_{Ic}}$ and the end notch flexure (ENF) test for measuring $\mathbf{G_{IIc}}$.

6.2 FATIGUE DAMAGE AND LIFE PREDICTION

Fatigue behaviour is usually expressed in terms of the maximum applied fatigue stress **S** and fatigue life (number of cycles to failure $\mathbf{N_f}$). This section examines four approaches to predicting fatigue performance of composite laminates (including statistical, fracture mechanics and empirical models).

6.2.1 Strength Degradation – Deterministic Approach

The residual strength, **S(N)**, initially equals the static strength $\boldsymbol{\sigma_{ULT}}$, and is assumed to monotonically decrease with fatigue cycles. Ignoring environmental and frequency effects, the rate of degradation should be dependent on $\boldsymbol{\sigma_{ULT}}$, the magnitude of the maximum stress $\boldsymbol{\sigma_{MAX}}$ and the stress ratio **R**.

The residual strength **S(N)** has been written in the form of [25]:

$$S(N) = \sigma_{ULT} - (\sigma_{ULT} - \sigma_{MAX})\left(\frac{N}{N_f}\right)^{v} \tag{43}$$

where **N** is the number of constant amplitude loading cycles before carrying out the residual strength test, $\mathbf{N_f}$ is the constant amplitude fatigue life and **v** is the "strength degradation parameter". Failure is assumed to occur when the residual strength **S(N)** is equal to the maximum stress $\boldsymbol{\sigma_{MAX}}$. The peak stress $\boldsymbol{\sigma_{MAX}}$ is usually 50% of $\boldsymbol{\sigma_{ULT}}$. Equation (43) defines a family of **S(N)** curves for residual strength as a function of fatigue loading cycles prior to strength testing. The path of each curve is dependent on the strength degradation parameter **v** with: (i) linear degradation occurring for $\mathbf{v = 1}$; (ii) sudden death behaviour for $\mathbf{v >> 1}$; and (iii) rapid initial loss of strength for $\mathbf{v < 1}$.

6.2.2 Strength Degradation - Statistical Approach

Due to the inherent variability in residual strength and life expectancy, the deterministic approach described in Section 6.2.2 has generally proved inaccurate, necessitating statistical analysis of the data. A widely used approach has been to represent the residual strength and life expectancy by two parameter Weibull functions. Using this approach, the probability of failure for constant amplitude loading (i.e. the probability that the residual strength after **N** cycles is less than the maximum applied stress $\boldsymbol{\sigma_{MAX}}$) can been expressed as [25]:

$$P[S(N) \le \sigma_{MAX}] = 1 - \exp\left[-\left(\frac{\sigma_{MAX}}{\sigma_{ULT} - (\sigma_{ULT} - \sigma_{MAX})\left(\frac{N}{N_f}\right)^{v}}\right)^{B_f(N)}\right] \tag{44}$$

where $\mathbf{B_f(N)}$ is the Weibull shape parameter for residual strength.

At zero cycles, Equation (44) should reduce to the static strength Weibull cumulative distribution function, which describes the probability that the initial strength $\mathbf{S_O}$ is less than or equal to the maximum stress $\boldsymbol{\sigma_{MAX}}$. This function has the following form [25]:

$$P[\sigma_{ULT} \le \sigma_{MAX}] = 1 - \exp\left[-\left(\frac{\sigma_{MAX}}{\sigma^{o}_{ULT}}\right)^{B_S}\right] \tag{45}$$

where $\mathbf{B_S}$ is the shape parameter for static strength and $\boldsymbol{\sigma^{o}_{ULT}}$ is a scaling parameter. Thus, a required scaling factor seems to be missing from Equation (44) and one might expect that $\mathbf{B_f(0) = B_s}$. Equation (44) predicts that $\mathbf{P[S(N_F) \le \sigma_{MAX}] = 1 - 1/e = 0.632}$ as $\mathbf{N \rightarrow N_f}$. This is a very peculiar result, as one would expect the probability to have some dependence on material properties. The identified problems relating to the use of Equation (44) seem to arise from substituting the deterministic relation given by Equation (43) for the residual strength in place of a required scaling factor.

A relation for the Weibull fatigue life distribution is given by [25]:

$$P[\,N_f \le N\,] = 1 - \exp\left[-\left(\frac{N}{N_f^o} \right)^{B_L} \right] \tag{46}$$

where $\mathbf{B_L}$ is the shape parameter for fatigue life and where $\mathbf{N_f^o}$ is a scaling parameter.

Static and fatigue life tests are conducted to obtain $\mathbf{N_f}$ and $\boldsymbol{\sigma_{ULT}}$, the shape parameters $\mathbf{B_f(N)}$, $\mathbf{B_L}$ and $\mathbf{B_S}$, and the scaling factors. The "optimum" value of the strength degradation parameter **v** is obtained by determining the best predictive fit of Equation (44) to the experimental data. The scatter in residual strength distributions increases with increasing cycles, and hence the shape parameter decreases.

6.2.3 Stress Transfer Model

Shear-lag models are being used to predict the damage progression and subsequent elastic property degradation of cross-ply laminates under monotonic and cyclic loading conditions. However, these models are empirical and tend to provide higher residual stiffness values than the experimental results. Dr L N McCartney at NPL has developed a stress transfer model, based on stress intensity factors (strain-energy release rates) for predicting the growth of pre-existing defects, and the effects of fatigue damage on the thermo-mechanical performance of $[0_m/90_n]$ cross-ply laminates. The model predicts ply crack formation in 90° plies and thermo-mechanical degradation in a cross-ply laminate during fatigue loading. An attempt to validate the physics/mechanistic model has shown that the first order approach leads to a conservative estimate of fatigue performance that can be exploited in the design of fatigue resistant composite laminates. It has been possible to predict the degradation of all non-shear properties of the laminate as a function of loading cycles. Details of the model and validation work can be obtained by contacting neil.mcartney@npl.co.uk.

6.3.3 Fracture Mechanics

Fracture mechanics is best suited to predicting failure subsequent to crack propagation along a parallel crack path. The general approach is to relate the crack growth rate **da/dt** through the composite to the applied strain-energy release rate **G** or the stress intensity factor **K**. Crack growth rate per loading cycle **da/dN** can be related to the maximum value of the applied strain-energy release-rate $\mathbf{G_{MAX}}$ by the form of the Paris Equation [23-24]:

$$\frac{da}{dN} = C(G_{MAX})^n \tag{47}$$

where **C** and **n** are material constants. This relationship applies only to the linear portion of the logarithmic-logarithmic plot of $\mathbf{G_{MAX}}$ versus **da/dN** (see Figure 8). Alternatively, the crack growth rate can be expressed as a function of the range of strain-energy release-rate $\boldsymbol{\Delta G}$ (see Equation (49)) by [23-24]:

$$\frac{da}{dN} = A(\Delta G)^q \tag{48}$$

where **A** and **q** are constants.

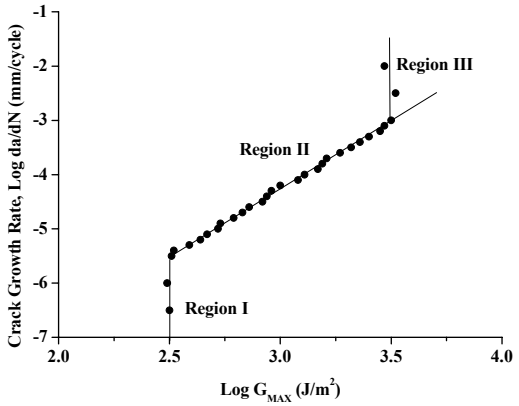

Regions

Region I – Threshold region ($\mathbf{G_{TH}}$) associated with low crack growth rate **da/dN** and $\mathbf{G_{MAX}}$ values ($\mathbf{G_{TH} \approx 0.1 G_C}$).

Region II – Linear region defined by the Paris Law given by Equation (47).

Region III – Value of $\mathbf{G_{MAX}}$ approaches the adhesive fracture toughness $\mathbf{G_c}$ measured under monotonic loading conditions.

Figure 8: Typical log-log crack growth rate versus G_{MAX} plot.

The difference between maximum and minimum strain-energy release-rate per cycle **ΔG** is given by:

$$\Delta G = G_{MAX} - G_{MIN} \tag{49}$$

This relationship only applies to the linear portion of the logarithmic-logarithmic plot of **ΔG** versus **da/dN**. Values for both sets of constants (i.e. **C** and **n**, and **A** and **q**) can be determined using linear regression fit to the linear region of the logarithmic-logarithmic plots.

Generally, the relationship between **log G_{MAX}** and **log ΔG** and **log da/dN** is S-shaped (i.e. sigmoidal). This relationship can be described as follows [26-27]:

$$\frac{da}{dN} = C\left(G_{MAX}\right)^n \left[\frac{1 - \left(\frac{G_{TH}}{G_{MAX}} \right)^{n_1}}{1 - \left(\frac{G_{MAX}}{G_c} \right)^{n_2}} \right] \tag{50}$$

$\mathbf{G_{TH}}$ is the minimum (or threshold) value of the adhesive fracture energy, $\mathbf{G_c}$, and **A**, **n**, $\mathbf{n_1}$ and $\mathbf{n_2}$ are material constants. $\mathbf{G_c}$ is determined from constant rate of displacement tests (i.e. monotonic fracture energy).

6.2.4 Empirical Approaches

A number of attempts have been made to empirically model stress-life behaviour of composites [22, 28-30]. Harris and co-workers [31-32] have developed a constant life-model (see Equation (51)), which according to the authors, agrees well with experimental data for tension-tension, compression-compression and tension-compression fatigue. The model is based on a substantial experimental database including results for different **R** ratios (stress ratio $\mathbf{R = \sigma_{MIN}/\sigma_{MAX}}$), constant and variable amplitude loading, materials (i.e. aramid, carbon and glass fibre-reinforced systems) and lay-ups, etc [33]. The model is claimed to account for both undamaged and damaged composite materials. Bell-shaped constant life diagrams are used to display the data.

The constant-life model is given by [31-33]:

$$a = f(1-m)^u (c+m)^v \qquad (51)$$

$$\text{where: } a = \frac{\Delta\sigma}{\sigma_{UTS}};\ \ m = \frac{\sigma_{MEAN}}{\sigma_{UTS}};\ \ c = \frac{\sigma_{UCS}}{\sigma_{UTS}}$$

The parameter **c** is the normalised compression strength (i.e. ratio of compressive strength, σ_{UCS}, to tensile strength, σ_{UTS}), **m** is the normalised mean stress component ($\sigma_{MEAN}/\sigma_{UTS}$) and **a** is the normalised stress amplitude ($\Delta\sigma/\sigma_{UTS}$). The parameters **f** (stress function), **u** and **v** in Equation (51) are linear functions of **log** N_f (N_f is the cycles to failure). This approach will be investigated in a future report on predictive models for characterising long-term behaviour of PMCs exposed to aggressive environments and cyclic fatigue loading conditions.

For unidirectional and cross-ply glass fibre-reinforced composites, the normalised **S-N** data for tension-tension fatigue can be represented by a linear relationship as follows [34]:

$$\sigma_{MAX} / \sigma_{UTS} = 1 - k \log_{10} N_f \qquad (52)$$

where σ_{MAX} is the maximum applied load, σ_{UTS} is the ultimate tensile strength, **k** (the slope) is the fractional loss in tensile strength per decade of cycles and N_f is the number of cycles to failure. The value of **k** is approximately 0.1 for the aligned materials and stress ratio **R = 0.1**. Increasing the mean load has a deleterious effect on the fatigue life. Similar behaviour has been observed for a wide range of fibre formats (with and without holes), wet and dry, room temperature and elevated temperatures [35-37].

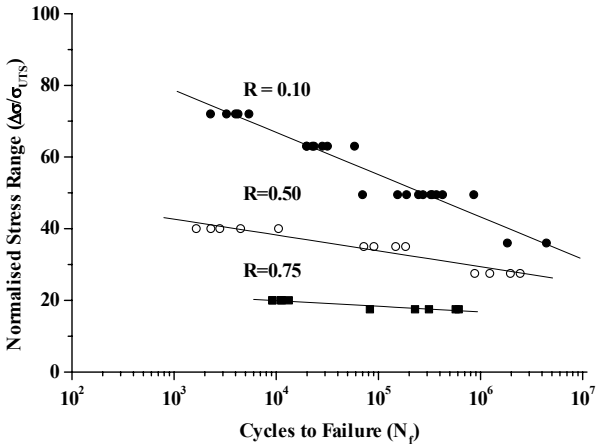

Figure 9: S-N curves for unidirectional E-glass/913 [34].

It has also been observed that the normalised **S-N** data (i.e. normalised maximum stress σ_{MAX} versus N_f) for three different stress ratios (0.1, 0.5 and 0.75) can be approximated by the linear relationship (see Figures 9 and 10) [34]:

$$k = 0.11 - 0.07R \qquad (53)$$

with the fractional loss in tensile strength per decade of cycles, **k**, decreasing as **R** increases.

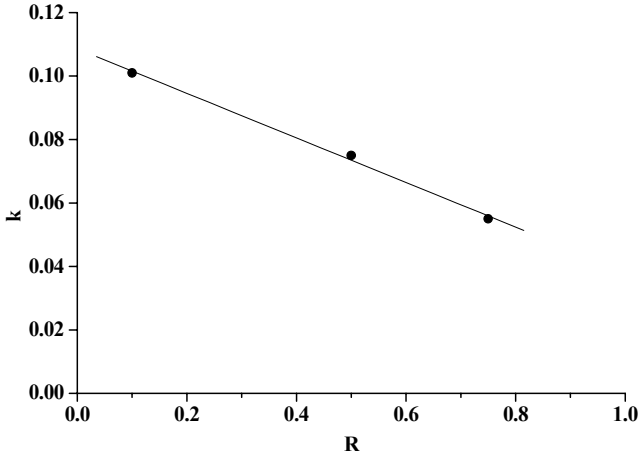

Figure 10: Plot of k as a function of R for unidirectional E-glass/913 [34].

6.3 CREEP BEHAVIOUR

Findley's power law model is widely used for describing the viscoelastic behaviour of composite materials under a constant (static) stress [38]. The model has been applied to a range of composite materials and has been included in the ASCE Structural Plastics Design Manual [39]. The time-dependent creep strain **ε(t)** is determined using [38]:

$$\varepsilon(t) = \varepsilon'_o + \varepsilon'_t t^n \tag{54}$$

where $\boldsymbol{\varepsilon'_o}$ is the stress-dependent and temperature-dependent initial elastic strain, $\boldsymbol{\varepsilon'_t}$ is the stress-dependent and temperature-dependent coefficient, **n** is a stress-independent material constant and **t** is the time after loading.

The terms $\boldsymbol{\varepsilon'_o}$ and $\boldsymbol{\varepsilon'_t}$ are often expressed as a polynomial series as shown below [38]:

$$\varepsilon'_o(\sigma, T) = a_1\left(\frac{\sigma}{\sigma_0}\right) + a_2\left(\frac{\sigma}{\sigma_0}\right)^2 + a_3\left(\frac{\sigma}{\sigma_0}\right)^3 + \ldots \tag{55}$$

$$\varepsilon'_t(\sigma, T) = b_1\left(\frac{\sigma}{\sigma_0}\right) + b_2\left(\frac{\sigma}{\sigma_0}\right)^2 + b_3\left(\frac{\sigma}{\sigma_0}\right)^3 + \ldots \tag{56}$$

Equation (54) can be rewritten in terms of creep compliance as follows:

$$D(t) = D_0 + D_t t^n \tag{57}$$

where **D(t)** is time-dependent creep compliance, **σ** is stress, $\mathbf{D_0}$ is the instantaneous creep compliance and $\mathbf{D_t}$ is the amplitude of transient creep compliance.

Findley's power law can also be used to derive expressions for time-dependent in-plane and through-thickness viscoelastic moduli of composite materials:

$$E_v = \frac{E_0 E_t}{E_t + E_0 t^n} \tag{58}$$

where $\mathbf{E_v}$ is viscoelastic modulus, $\mathbf{E_0}$ is initial modulus and $\mathbf{E_t}$ characterises time dependent behaviour.

7. CONCLUDING REMARKS

The large number and diversity of materials models and failure criteria in the published literature (with no evidence of a slow-down) indicates that there is still a major concern as to the suitability of these different approaches for design purposes. Although this comment applies equally to adhesives and composite materials, the complexity of composite materials adds another dimension to this difficult task. This is best demonstrated by the comparative exercise being carried out by Dr M Hinton at QinetiQ (formerly DERA) into the comparative capabilities of current failure theories for composite laminates (see [40-41]). This was an international exercise involving all key proponents in the field. Final conclusions are still to be drawn, but early evidence suggests that there is no theory that can be applied to all systems and loading conditions.

It is intended that a number of modelling approaches will be examined within MMS 11 "Design for Fatigue and Creep in Joined Systems" to ascertain their suitability and ease of implementation in FEA and analytical design packages (i.e. CoDA) for bonded and bolted metallic and composite structures. It is intended to evaluate a number of these approaches through the use of case studies in the form of aluminium and composite Tee joints that will be either adhesively bonded or bolted. These joints will be subjected to direct tensile or lateral loads under monotonic, creep and fatigue loads. Static strength, progressive damage formation, the time-to-failure and the time dependence of residual strength of the joined structures will be compared with predictive analysis.

A new model for characterising the behaviour of rubber-toughened adhesives, which accounts for the influence of rubber particle cavitation on the yield behaviour of adhesives will be used in conjunction with FEA to determine the response of aluminium and composite single-lap, scarf, T-peel and Tee joints. This work will be extended to modelling non-linear creep behaviour in bulk adhesives and adhesive joints through the use of a model for time-dependent plasticity.

ACKNOWLEDGEMENTS

This work forms part of the extension programme for "Measurements for Materials Systems" funded by the Engineering Industries Directorate of the UK Department of Trade and Industry, as part of its support of the technological competitiveness of UK industry. The authors would like to express their gratitude to all members of the Industrial Advisory Group (IAG) and to colleagues at the National Physical Laboratory, particularly to Dr Louise Crocker.

REFERENCES

1. Gurson, A.L., "Continuum Theory of Ductile Rupture by Void Nucleation and Growth: Part 1 – Yield Criteria and Flow Rules for Porous Ductile Media", Journal of Engineering Materials Technology, Transactions of ASME, Volume 99, 1977, pp 2-15.
2. "Physics of Glassy Polymers", Second Edition, Edited by Haward, R.N. and Young, R.J., Chapman and Hall, London, 1997.
3. Lazzeri, A. and Bucknall, C.B., "Dilatational Bands in Rubber-Toughened Polymers", Journal of Materials Science, Volume 28, 1993, pp 6799-6808.
4. Hart-Smith, L.J., "Adhesive-Bonded Single-Lap Joints", NASA Report CR-112236, 1973.
5. Hart-Smith, L.J., "Adhesive-Bonded Scarf and Stepped-Lap Joints", NASA Report CR-112237, 1973.
6. Hart-Smith, L.J., "Adhesive-Bonded Double-Lap Joints", NASA Report CR-112238, 1973.
7. Hart-Smith, L.J., "Analysis and Design of Advanced Composite Bonded Joints", NASA Report CR-2218, 1974.
8. Harris, J.A. and Adams, R.D., "Strength Prediction of Bonded Single Lap Joints by Non-Linear Finite Element Methods", International Journal of Adhesion and Adhesives, Volume 4, Number 2, 1984, pp 65-78.
9. Adams, R.D., "The Mechanics of Bonded Joints, Structural Adhesives in Engineering, ImechE Conference Publications, Suffolk, 1986, pp 17-24.
10. Tong, L. and Steven, G.P., "Analysis and Design of Structural Bonded Joints", Kluwer Academic Publishers, 1999.
11. Read, B.E., Dean, G.D. and Ferriss, D.H., "An Elastic-Plastic Model for the Non-Linear Mechanical Behaviour of Rubber-Toughened Adhesives", NPL Report CMMT(A)289, 2000.
12. Dean, G.D. and Crocker, L., "Comparison of the Measured and Predicted Deformation of an Adhesively Bonded Lap-Joint Specimen", NPL Report CMMT(A)293, 2000.
13. Broughton, W.R., Crocker, L.E. and Urquhart, J.M., "Strength of Adhesive Joints: A Parametric Study", NPL Report MATC(A)27, 2001.
14. Dean, G. and Crocker, L., "The Use of Finite Element Methods for Design with Adhesives", NPL Measurement Good Practice Guide No 48, 2002.
15. Military Handbook Polymer Matrix Composites, Volume 3 – Materials Usage, Design and Analysis, MIL-HDBK-17-1E.
16. Whitcomb, J. and Noh, J., "Concise Derivation of Formulas for 3D Sublaminate Homogenization", Journal of Composite Materials, Volume 34, Number 06, 2000, pp 523-535.
17. Jones, R.M., "Mechanics of Composite Materials", Hemisphere Publishing Corporation, 1975.
18. Hill, R., "The Mathematical Theory of Plasticity", Oxford University Press, London, UK, 1950.

19. Azzi, V.D., and Tsai, S.W., “Anisotropic Strength Components”, Experimental Mechanics, Volume 5, 1965, pp 283-288.
20. Tsai, S.W. and Wu, E.M., “A General Theory of Strength for Anisotropic Materials”, Journal of Composite Materials, Volume 5, 1971, pp 58-80.
21. Wu, Ru-Yu. and Stachurski, Z., "Evaluation of the Normal Stress Interaction Parameter in the Tensor Polynomial Strength Theory for Anisotropic Materials" Journal of Composite Materials, 18, 1984, pp 456-463.
22. Broughton, W.R. and McCartney, L.N., “Predictive Models for Assessing Long-Term Performance of Polymer Matrix Composites”, NPL Report CMMT(A)95, 1998.
23. Kinloch, A.J. and Osiyemi, S.O., “Predicting Fatigue Life of Adhesively-Bonded Joints”, Journal of Adhesion, Volume 43, 1993, pp 79-90.
24. Curley, A.J., Hadavinia, H., Kinloch, A.J. and Taylor, A.C., “Predicting the Service-Life of Adhesively-Bonded Joints”, International Journal of Fracture, Volume 103, 2000, pp 41-69.
25. Schaff, J.R. and Davidson, B.D., “Life Prediction Methodology for Composite Structures. Part I - Constant Amplitude and Two-Stress Level Fatigue”, Journal of Composite Materials”, Volume 31, Number 2, 1997, pp 128-157.
26. Fernlund, G., Papini, M., McCammond, D. and Spelt, J.K., “Fracture Load Predictions for Adhesive Joints”, Composites Science and Technology, Volume 51, 1994, pp 587-600.
27. Ashcroft, I.A, Gilmore, R.B and Shaw, S.J., “Cyclic Fatigue and Environmental Effects with Adhesively Bonded Joints”, AGARD 83rd SMP Meeting, Florence, 1996.
28. Talreja, R., `Statistical considerations', Chapter 11, "Fatigue of Composite Materials", Editor, Reifsnider, K.L., Elsevier Science Publishers, Amsterdam-Oxford-New York-Tokyo, 1990.
29. Shokrieh, M.M. and Lessard, L.B., “Progressive Fatigue Damage Modeling of Composite Materials, Part I: Modeling”, Journal of Composite Materials, Volume 34, Number 13, 2000, pp 1056-1080.
30. Shokrieh, M.M. and Lessard, L.B., “Progressive Fatigue Damage Modeling of Composite Materials, Part II: Material Characterization and Verification”, Journal of Composite Materials, Volume 34, Number 13, 2000, pp 1081-1116.
31. Gathercole, N., Reiter, H., Adam, T. and Harris, B., “Life Prediction for Fatigue of T800/5435 Carbon-Fibre Composites: 2 Constant Amplitude Loading, Fatigue Journal, Volume 16, 1994, pp 523-532.
32. Gathercole, N., Reiter, H., Adam, T. and Harris, B., “Life Prediction for Fatigue of T800/5435 Carbon-Fibre Composites: 2 Variable Amplitude Loading, Fatigue Journal, Volume 16, 1994, pp 533-547.
33. Curtis, P.T., “Designing for Fatigue and Environmental Effects in Polymer Composites”, “International Conference on Designing Cost-Effective Composites, IMechE Conference Transactions, London, UK, 1998, pp 53-63.
34. Broughton, W.R., and Lodeiro, M.J., “Fatigue Testing of Composite Laminates”, NPL Report CMMT(A)252, 2000.
35. Sims, G.D. and Gladman, D.G., “Effect of Test Conditions on the Fatigue of a Glass-Fabric Laminate: Part A- Frequency”, Plastics and Rubber: Materials and Applications, May 1978, pp 41-48.
36. Sims, G.D. and Gladman, D.G., “Effect of Test Conditions on the Fatigue of a Glass-Fabric Laminate: Part B- Specimen Condition”, Plastics and Rubber: Materials and Applications, August 1980, pp 122-128.
37. Mandell, J.F., Huang, D.D. and McGarry, F.T., “Tensile Fatigue Performance of Glass-Fiber-Dominated Composites”, Composites Technology Review, Volume 3, Number 3, 1981, pp 96-102.

38. Scott, D.W., Lai, J.S. and Zureick, A-H., “Creep Behaviour of Fiber-Reinforced Polymeric Composites: A Review of the Technical Literature”, Journal of Reinforced Plastics and Composites, Volume 14, 1995, pp 588-617.
39. “Structural Plastics Design Manual”, American Society of Civil Engineers, ASCE Publications, 1984.
40. Hinton, M.J. and Soden, P.D., “Predicting Failure in Composite Laminates: The Background to the Exercise”, Composite Science and Technology, Volume 8, Issue Number 7, 1998, pp 1011-1022.
41. Soden, P.D., Hinton, M.J. and Kaddour, A.S., “A Comparison of the Predictive Capabilities of Current Failure Theories for Composite Laminates”, Composite Science and Technology, Volume 8, Issue Number 7, 1998, pp 1225-1254.

APPENDIX 1. FINITE ELEMENT ANALYSIS CONTOUR PLOTS

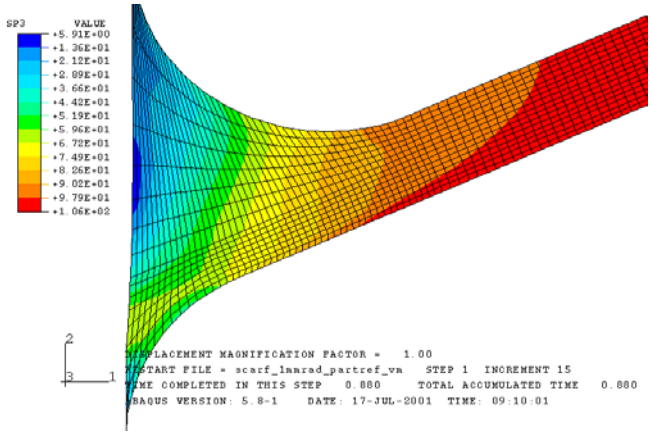

von Mises analysis

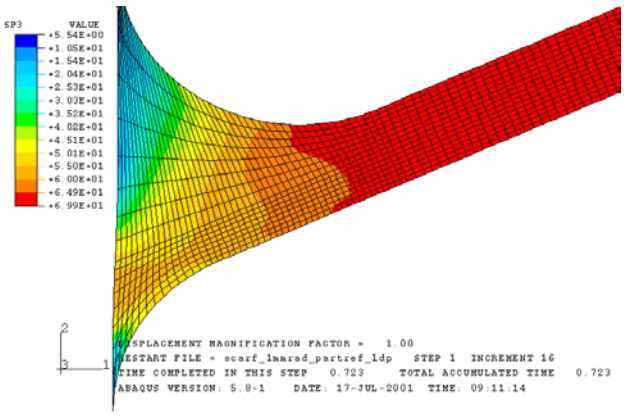

Linear Drucker-Prager analysis

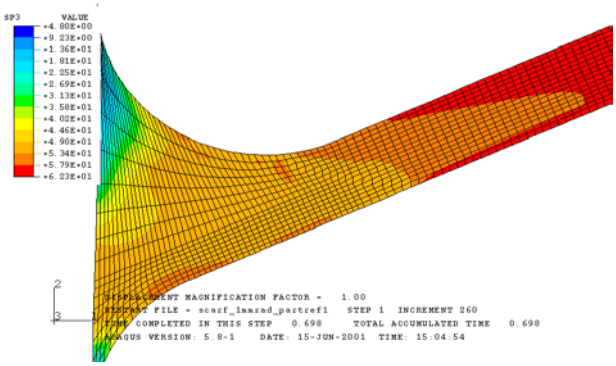

Exponent Drucker-Prager analysis

Figure A1.1: Contour plots of maximum principal stress in the adhesive at an extension of 0.035 mm obtained from analyses using three different material models.

APPENDIX 1. FINITE ELEMENT ANALYSIS CONTOUR PLOTS

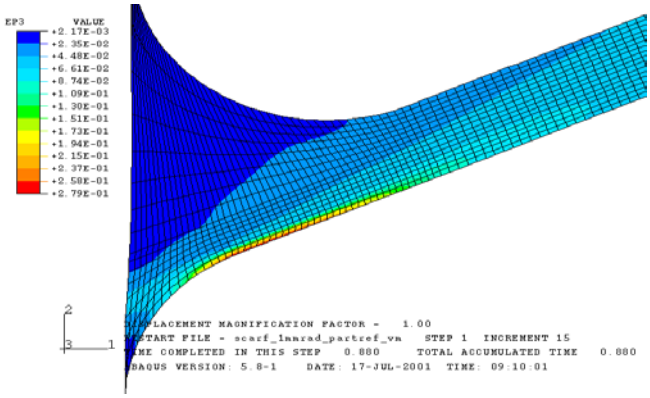

von Mises analysis

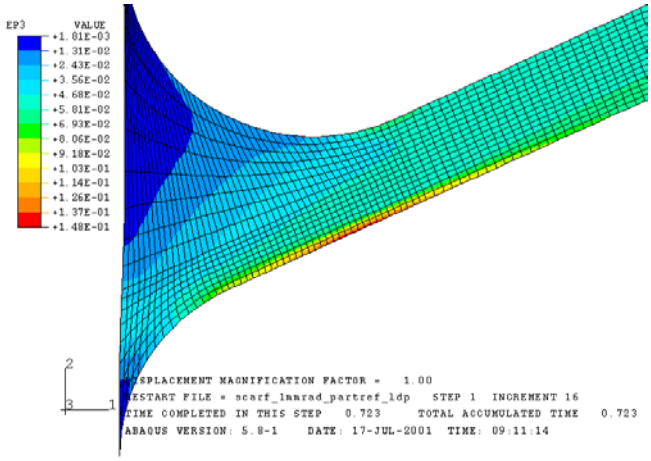

Linear Drucker-Prager analysis

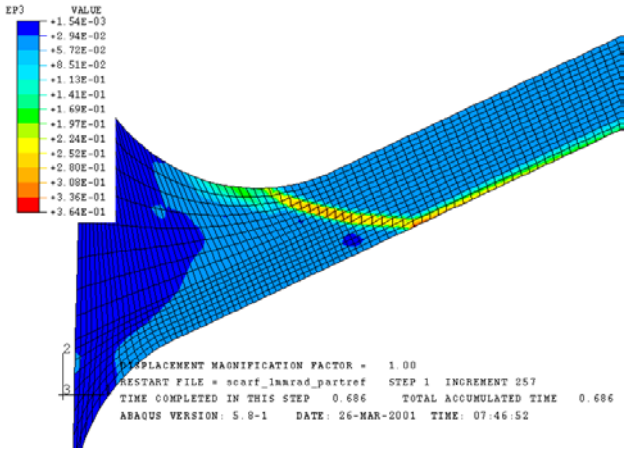

Exponent Drucker-Prager analysis

Figure A1.2: Contour plots of maximum principal strain in the adhesive at an extension of 0.035 mm obtained from analyses using three different material models.